Satellite multi-sensor mapping of suspended particulate matter in turbid estuarine and coastal ocean, China

Fang Shen[a], Yunxuan Zhou[a], Xiangyi Peng[a] & Yuli Chen[a]

[a] State Key Laboratory of Estuarine and Coastal Research, East
China Normal University, Shanghai 200062, China
Published online: 05 Jun 2014.

PLEASE SCROLL DOWN FOR ARTICLE

Taylor & Francis
Taylor & Francis Group

Satellite multi-sensor mapping of suspended particulate matter in turbid estuarine and coastal ocean, China

Fang Shen*, Yunxuan Zhou, Xiangyi Peng, and Yuli Chen

State Key Laboratory of Estuarine and Coastal Research, East China Normal University, Shanghai 200062, China

In this work, five ocean-colour sensors, the Moderate Resolution Imaging Spectroradiometer aboard the Terra satellite (Terra MODIS), Moderate Resolution Imaging Spectroradiometer aboard the Aqua satellite (Aqua MODIS), Medium Range Imaging Spectrometer aboard the Environmental Satellite (Envisat MERIS), Medium Resolution Spectral Imager aboard the FY-3 satellite (FY-3 MERSI), and Geostationary Ocean Colour Imager (GOCI), were selected to examine the compatibility of an algorithm proposed for suspended particulate matter (SPM) retrieval and concordance of satellite products retrieved from different ocean-colour sensors. The results could effectively increase revisit frequency and complement a temporal gap of time series satellites that may exist between on-orbit and off-orbit. Using *in situ* measurements from 17 cruise campaigns between 2004 and 2012, the SPM retrieval algorithm was recalibrated so as to be universal and adapted for multi-sensor retrievals. An inter-comparison of multi-sensor-derived products showed that GOCI-derived SPM and Envisat MERIS-derived SPM had the best fitting on a 1:1 scatterplot, with a statistic regression slope of 0.9617 and an intercept of 0.0041 (in units of g l^{-1}), respectively. SPM products derived from three sensors with nearly synchronous transit, Envisat MERIS, Terra MODIS, and FY-3 MERSI, exhibited excellent accordance with mean differences of 0.056, 0.057, and 0.013 g l^{-1} in three field fixed stations, respectively, in the Yangtze estuary. Terra MODIS-derived SPM with GOCI-derived SPM, except in the high SPM waters of Hangzhou Bay, and Aqua MODIS-derived SPM with GOCI-derived SPM, except in the moderate SPM waters of the South Branch and south of the Subei Coast, showed a good correspondence. Meanwhile, synchronous multi-sensor-derived SPM with concurrent *in situ* SPM time series observed in fixed field stations mostly displayed a good correspondence. Results suggest that the algorithm is feasible and compatible for SPM retrieval by multiple sensors.

1. Introduction

Suspended particulate matter (SPM) not only plays an important role in the construction and evolution of estuarine, coastal, and continental geomorphology, and harbour and dredging engineering of navigation channels (El-Asmar and White 2002), but also has significant impacts on estuarine, coastal water quality, and ecosystems (Schoellhamer, Mumley, and Leatherbarrow 2007). Light attenuation due to the presence of SPM in the water affects phytoplankton photosynthesis (Krause-Jensen and Sand-Jensen 1998), which is closely associated with marine ecology and biogeochemistry. This interaction between land and ocean in turbid coastal waters, e.g. in the Yellow Sea and East China Sea, is also a key research topic (Figure 1(*a*)).

---

*Corresponding author. Email: fshen@sklec.ecnu.edu.cn

(*a*) **FY-3 MERSI RGB composite of 686, 565 and 443 nm**   (*b*) **FY-3 MERSI retrieved SPM concentration**

(*c*) **Location map of fixed stations in the Yangtze estuary**
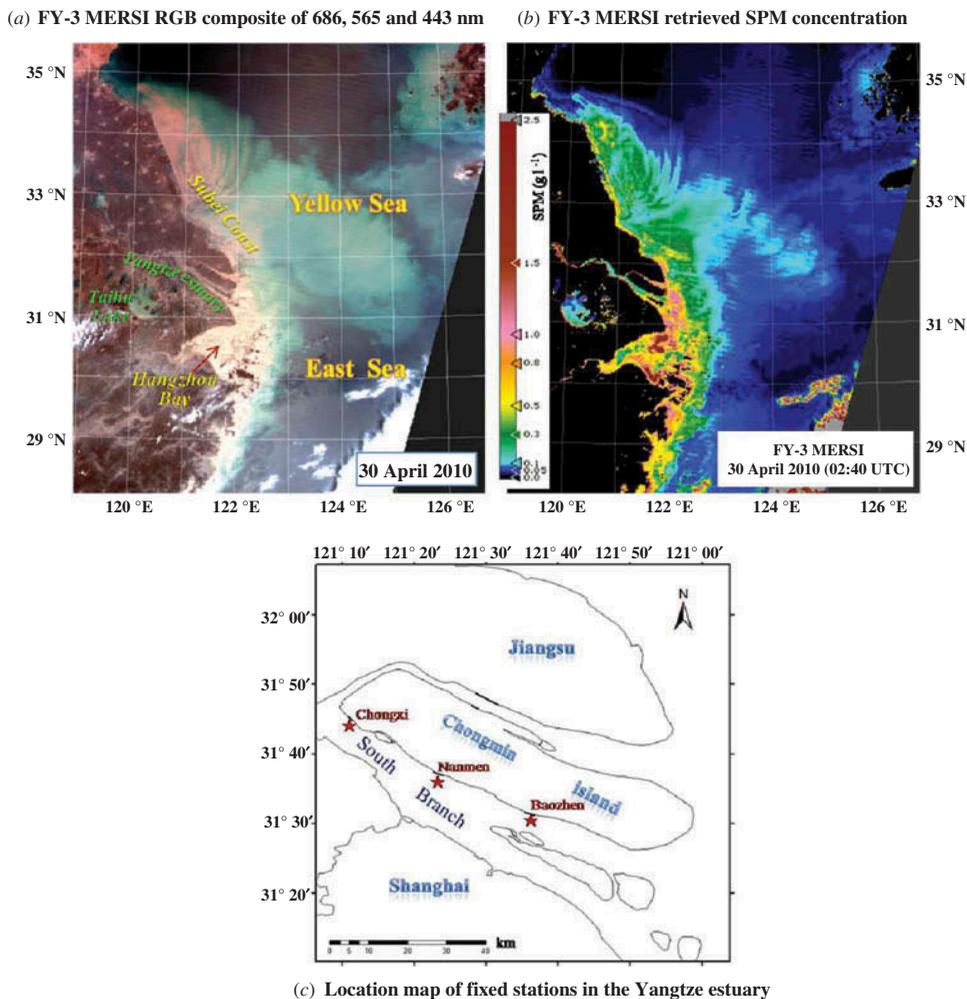
Figure 1.   Maps of the study area. (*a*) FY-3 MERSI RGB composite of 686, 565 and 443 nm; (*b*) FY-3 MERSI retrieved SPM concentration; (*c*) location map of fixed stations in the Yangtze estuary.

Ocean satellite observations have achieved remarkable results since ocean-colour sensors were successively launched (McClain 2009), with 13 sensors functioning between 1996 and 2011 and eight polar-orbiting ocean-colour sensors currently in orbit (http:// ioccg.org/sensors/). To achieve a sustainable understanding of the effects of climate change on the global ocean environment and ecosystem, an advance development of the next generation of ocean-colour missions has been planned and 10 more polar-orbiting ocean-colour sensors have been scheduled (http://ioccg.org/sensors/). An effort to merge the data products from several sensors has been made (Gregg and Woodward 1998; Maritorena and Siegel 2005; Pottier et al. 2006; Maritorena et al. 2010), and in recent years the consistency of multiple sensor products in case-1 waters has been examined (Morel et al. 2007). The benefits of such work can increase spatial and temporal coverage in ocean observations and complement a temporal gap of time series of satellites that may

exist between on-orbit and off-orbit. Moreover, blended multi-sensor products can enhance matchup probability (IOCCG 2007).

The objective of this work was to examine the compatibility of an algorithm we developed for SPM retrieval and the concordance of the retrieved products using satellite data from different ocean-colour sensors. Five ocean-colour sensors, the Moderate Resolution Imaging Spectroradiometer aboard the Terra satellite (Terra MODIS), Moderate Resolution Imaging Spectroradiometer aboard the Aqua satellite (Aqua MODIS), Medium Range Imaging Spectrometer aboard the Environmental satellite (Envisat MERIS), Medium Resolution Spectral Imager aboard the FY-3 satellite (FY-3 MERSI), and Geostationary Ocean Colour Imager (GOCI), were selected for this objective. An effort was made in this work to expand the application of Chinese satellites, e.g. the SPM retrieved using FY-3 MERSI data (see Figure 1(*b*)) as well as to compare inter-sensor products. The motivation for this originated from the mapping of SPM products from FY-3 MERSI, which have rarely been published in official websites and literature. Although FY-3 is a meteorological satellite, the MERSI sensor as its payload can be suitable for ocean applications because of its bands that are specially designed for ocean colour (details in Section 2.1).

2. Satellite data and *in situ* data

2.1. *Ocean colour sensors*

Ocean-colour sensors are designed to retrieve the spectral distribution of upwelling radiance just above the sea surface (the water-leaving radiance), which is then used to estimate a number of geophysical parameters (IOCCG 2008). Because less than 10% of the radiance measured originates from the water components, ocean-colour sensors require a high signal-to-noise ratio. The quantitative estimation of water components and concentrations, and even biogeochemical variables, in the optically complex coastal waters demands an elaborate and large number of spectral bands (IOCCG 2000). Moreover, monitoring estuarine and coastal areas needs remote-sensing data with high spatial resolution. The high variability of the estuarine and coastal environment due to short time-scale tidal variations promotes the ocean-colour community to develop geostationary ocean-colour satellite missions with high-frequency observations. In this work, considering the prevalence of ocean-colour products and applications, satellite data for SPM retrieval from four on-orbit sensors – polar (Terra MODIS, Aqua MODIS, and FY-3 MERSI) and geostationary (GOCI) – and from the Envisat MERIS (which recently died) were chosen. The characteristics of the five sensors are listed in Table 1.

The two MODIS instruments, respectively mounted on the Terra (1999–present) and Aqua (2002–present) satellites, with three modes of spatial resolution of 250, 500, and 1000 m, can be programmed to conduct measurements around 10:30 local time (crossing time of Terra) and 13:30 (crossing time of Aqua). The MODIS sensor is designed to have 36 bands covering a spectral range from 0.4 μm (visible) to 14.4 μm (thermal infrared), among which there are two bands with a spatial resolution of 250 m that are more suitable for estuarine and coastal applications.

MERIS, which was initially designed for coastal applications, mounted on the Envisat satellite (2002–2012), was launched by the European Space Agency (ESA) with a full and reduced spatial resolution of 300 and 1200 m and 1–3 day revisit time. Its full resolution and 15 elaborate ocean-colour band settings have special abilities to observe optically complex estuarine, coastal, and inland waters. The Sentinel-3 Ocean

Table 1. Features of five ocean-colour sensors.

Granule features	Terra/aqua MODIS	Envisat MERIS	FY-3 MERSI	GOCI
Orbit	Polar	Polar	Polar	Geostationary
Altitude (km)	705	800	836	35,786
Swath (km)	2330	1150	2400	2500
Ocean bands & other bands (nm)	1 km: 412, 443, 488, 531, 551, 667, 678, 748, 869; 250 m: 654, 858	412, 443, 490, 510, 560, 620, 665, 681, 709, 779, 865	1 km: 412, 443, 490, 520, 565, 650, 685, 765, 865; 250 m: 470, 550, 650, 865, 1125	412, 443, 490, 555, 660, 680, 745, 865
SNR range	750 to 1087	> 500	NE$\Delta\rho$: 0.05%	750–1000
Revisit	2 day (a.m./p.m.)	1–3 day	1–3 day	8 day (1 hour interval)
Spatial resolution (m)	250/500/1000	300/1200	250/1000	500

and Land Colour Instrument (OLCI) is a continuity of the MERIS capability and is expected to be launched in 2014. The OLCI marks a new generation of measurements over oceans and land, with improvements in an increased number of spectral bands (from 15 to 21), mitigation of sunglint contamination, and complete coverage over oceans at 300 m (Donlon et al. 2012).

MERSI was installed on FY-3A (2008–present) and FY-3B (2010–present) Chinese polar-orbiting meteorological satellites (http://fy3.satellite.cma.gov.cn/) with a spatial resolution of 250 and 1000 m. It has 19 spectral bands covering 0.41 to 2.13 μm and one thermal infrared band centred at 11.25 μm, among which five bands (including four visible bands and one thermal infrared band) are with 250 m resolution, and 15 bands (nine ocean bands and six other bands) with 1000 m resolution (Sun et al. 2012).

The GOCI (2010–present), launched by the Korea Ocean Satellite Centre, is the first ocean-colour instrument mounted on a geostationary-orbiting Communication Ocean and Meteorological Satellite in the world at present (Choi et al. 2012). It scans a fixed ground area of 2500 km × 2500 km with the spatial coverage centred in the geographic coordinates of 36° N and 130° E (Ryu et al., 2012). The GOCI has eight spectral bands covering the visible to near-infrared spectral range with a spatial resolution of 500 m. The unique feature of the GOCI is its high frequency revisit time (1 hour interval), eight times per day from 00:15 UTC to 07:45 UTC. Hence, it is particularly appropriate for observing sediment transportation and ecosystem dynamics in estuaries and coasts.

2.2. Multi-sensor ocean colour products

MODIS level 1 products by region-of-interest or band were obtained from the NASA website (http://ladsweb.nascom.nasa.gov/) of the Level 1 and Atmosphere Archive and Distribution System (LAADS). Two data products of the MODIS level 1 – MOD02 from the MODIS Terra and MYD02 from the MODIS Aqua – contain the top of atmosphere (TOA) radiance calibrated. As a trade-off of relatively lower spectral resolution, the satellite data product of a relatively higher spatial resolution is able to depict clearly the heterogeneity of SPM spatial distribution in small-sized estuaries and mitigate contamination by neighbouring land pixels, and is therefore more suitable for estuarine SPM retrieval. Two spectral bands with full spatial resolution (250 m) – one in the visible

band (620–670 nm) and another in the near-infrared band (841–876 nm) – are available to be applied in SPM concentration retrieval in highly reflective estuarine and coastal waters (Miller and McKee 2004; Doxaran et al. 2009). Thus, the products MOD02QKM and MYD02QKM were selected. In addition, for the MOD03 and MYD03 products that include geographic coordinate information, solar zenith and azimuth angles are needed for the performance of data processing.

The archived Envisat MERIS level 1b products were provided by the ESA data service section through the joint programme ('Dragon Programme') of MOST (Ministry of Science and Technology of China) and ESA. The MERIS full resolution (FR) data are usually required to be ordered by users in advance, and have a limited amount of coverage due to confined ground receiver stations. MERIS reduced resolution (RR) data are relatively more popular. The MERIS level 1b products include TOA radiance, latitude and longitude, solar zenith and azimuth angles, flags system, and other ancillary data, which can be accessed and analysed through the BEAM VISAT software system developed by Brockmann Consulting, Inc. (http://www.brockmann-consult.de/beam/). We developed a turbid water SPM processor, which is an operational and updatable BEAM module under the Graph Processing Framework. The processor is more suitable for SPM retrieval in highly turbid waters, such as in the Yangtze estuarine and adjacent coastal waters. Performance of the processor involves two steps: the first is for deriving the atmospherically corrected water-leaving reflectance from the MERIS TOA radiance and the second is for the SPM inversion from the water-leaving reflectance. The processor was released to the Dragon-2 training course of Ocean Remote Sensing in 2011.

FY-3 MERSI products are attainable by application or registration to the Chinese Meteorological Satellite Centre (http://fy3.cma.gov.cn/). As far as compatibility is concerned, the FY-3 MERSI data format adopts the Hierarchical Data Format (HDF), which is the standard data format for all NASA Earth Observing System (EOS) data products. After radiometry calibration and georeference processing, two datasets of the MERSI level 1 (L1) product are generally used: MERSI_L1 250 m (five spectral bands with a spatial resolution of 250 m) and MERSI_L1 1000 m (15 spectral bands with a spatial resolution of 1000 m). The dataset MERSI_L1 1000 m is preferred for SPM retrieval as it includes data for nine ocean-colour bands.

GOCI Level 1b products were obtained from the Korea Ocean Satellite Centre (KOSC) in 2011 from April to December at the rate of eight images per day. The GOCI level 1b products were generated through preprocessing for raw data. Preprocessing includes the processes of radiometric correction from digital number to TOA radiance and preliminary geometric correction based on orbit information, satellite position, and landmark matching (Yang and Song 2012). Thereafter, the TOA radiance and georeferenced data in HDF format can be accessed and exported from the GOCI Data Processing Software (GDPS).

2.3.   In situ *cruise and fixed station data and matchups*

There were 17 cruise campaigns of *in situ* radiometric measurements and simultaneous water samplings carried out in distinct meteorological seasons each year from 2004 to 2012 in the Yangtze estuary and adjacent coastal ocean. In total, 225 samples of *in situ* radiometric measurements were collected.

Radiometric measurements were recorded using a system of HyperSAS spectroradiometers (Satlantic Inc.) designed for above-water measurements of ocean colour. The system consists of two radiance sensors and one irradiance sensor with 136 channels

covering the spectral range from 350 to 900 nm. Three sensors mounted to the SAS platform follow the specific observation geometry as recommended by the NASA protocols (Fargion and Muller 2000). One radiance sensor is pointed to the sea to measure the total radiance above the water (L_{tot}), while the other is pointed to measure the sky radiance (L_{sky}) necessary for sunglint correction. The sea and sky radiance sensors are pointed at the same nadir and zenith angles (between 30° and 50° with an optimum angle of 40°), respectively. To minimize the sunglint effects, the sea sensor is pointed at the azimuth angle between 90° and 180° away from the solar plane, with an optimum angle of 135° away from Sun. The irradiance sensor is used to measure the downwelling irradiance. Therefore, the remote-sensing reflectance (R_{rs}) is determined by the ratio of water-leaving radiance ($L_{tot}-\rho L_{sky}$) and downwelling irradiance (E_d), where ρ is the sea surface reflectance factor (Mobley 1999).

The SPM concentration was determined gravimetrically in laboratory. Water samples were filtered by 0.7 μm Whatman GF/F glass fibre filters. The blank and sample-filled filters were rinsed with Milli-Q water to remove salts, dried, and then reweighed on a high-precision balance in laboratory.

In this work, autonomous measurements for turbidity in units of NTU by D&A Tech optical backscatter instrument (OBS), at two minute intervals, at three fixed field stations, i.e. the Chongxi, Nanmen, and Baozhen stations (see Figure 1(*c*)), in the Yangtze mouth, had been collected since 2010. Generally, the OBS turbidity (NTU) may be transformed into the SPM concentration (g l^{-1}) by a calibrated relationship. The best approach for calibrating the OBS turbidity is to collect water samples immediately adjacent to the sensor and build a numerical relationship between the OBS signals and the SPM concentration of the samples (Downing 2006). However, it is less feasible to calibrate the OBS autonomous measurements. As an alternative approach, we adopted results of *in situ* OBS measurements with simultaneous water samplings from a cruise campaign in the Yangtze mouth during 2–3 July 2011. The OBS turbidity (defined by x) and the SPM concentration (defined by y) obeyed a linear regression relation: $y = 0.001x - 0.07$, with $R^2 = 0.935$, $n = 17$, and $p < 0.001$. Furthermore, considering the impact from size distribution of suspended particles on the OBS measurements, we also employed the calibration relationship developed by Xue, He, and Wang (2004), i.e. $y = 0.0017x + 0.0202$, which was based on the OBS measurements with simultaneous water samplings in the South Branch where the fixed stations are located. Thus, the mean values and deviations of the SPM derived from the OBS measurements through the two calibration relationships were estimated.

Three cloud-free days of 5 April and 9 October 2011 and 30 April 2010 were favoured as candidates of the matchups of the OBS turbidity and coincident multi-sensor-derived SPM products. We collected the OBS turbidity data in the three fixed stations on 5 April and 9 October 2011 and 30 April 2010. However, it failed to obtain the data in the Chongxi station on 5 April 2011 and on 9 October 2011 as well as in the Nanmen station on 9 October 2011, due to record failures of the OBS instruments. Ten images were captured on 5 April 2011, eight for GOCI (between 00:16 UTC and 07:40 UTC), one for Terra MODIS (02:20 UTC), and one for Aqua MODIS (05:35 UTC). There were nine images on 9 October 2011, eight for GOCI, and one for MERIS (02:20 UTC). On 30 April 2010, Terra MODIS (02:45 UTC), Envisat MERIS (02:04 UTC), and FY-3 MERSI (02:40 UTC) were almost concomitant. The matchups made it possible to examine the compatibility of the retrieval algorithm and the consistency of the multi-sensor SPM products.

3. Data processing

3.1. Reprojection

MODIS, MERIS, and MERSI and GOCI level 1 products obtained were data processed by radiometric correction, i.e. from digital number converted into TOA radiance, and preliminary geometric correction based on orbit attitude and satellite position. The region-of-interest of satellite scenes was tailored to the Yellow sea and the East China Sea. The georeferenced data from multiple sensors were tied to a fixed grid since MODIS, MERIS, MERSI, and GOCI have different scan footprints. The level 1 products in HDF format were transformed to the TIFF format by the IDL programs we developed and then imported into the BEAM software. Files were saved as BEAM-DIMAP of a self-defined format. It is possible to process data from MERIS and other sensors, and functions including display, analysis, and processing. The data reprojection in a unified georeference system and resampling operations were implemented due to different spatial resolutions in the BEAM. The reprojection facilitates inter-sensor product comparisons and integrated analysis (Ruddick et al. 2012). The function of collocation performed in BEAM made it available for comparative analysis and scatterplot mapping.

3.2. Supplement of look-up-tables

Significant progress in atmospheric correction of ocean colour data has been made in dealing with cases for absorbing aerosols and waters with non-negligible near-infrared ocean contributions (IOCCG 2010). For example, Wang, Son, and Shi (2009) proposed using the shortwave infrared (SWIR) bands for an atmospheric correction algorithm over coastal waters; Neural network approaches (Jamet et al. 2005; Brajard et al. 2006) were applied to atmospheric correction over case-2 coastal waters. Results from these approaches show an improvement in retrieval accuracy of water-leaving reflectance, e.g. in the Baohai Sea (Cui et al. 2010) and European coastal waters (Schroeder et al. 2007), etc. For extremely turbid waters such as the Yangtze mouth and Hangzhou Bay (SPM > 800 mg l^{-1}), however, current atmospheric correction approaches still present challenges. MODIS, MERIS, and GOCI atmospheric correction usually masks out highly turbid pixels of the Yangtze mouth and Hangzhou Bay. However, developing or improving an algorithm of atmospheric correction is beyond the scope of this article. Based on our previous work (Shen et al. 2010; Shen and Verhoef 2010), the approach of the look-up-tables (LUTs) was adopted for atmospheric correction. The atmospheric radiative transfer model (e.g. MODTRAN) was employed for creating the LUTs simulated by various atmospheric conditions, aerosol types, and Sun-view geometries, in the absence of measured atmospheric composition data and meteorological data over the study area at the moment of satellite overpass. The pre-generated LUTs included atmospheric visibilities of 5, 10, 20, and 40 km. The candidate aerosol types were maritime, rural, desert, urban, tropical, and Navy maritime with an air mass character of 3 (default value). The zenith angles of Sun and viewing, respectively, varied from 0° to 70° (5° interval), and the relative viewing azimuth varied over the angles of 0°, 45°, 90°, 135°, and 180°. Atmospheric components such as CO_2, water vapour, and ozone gas were set to 380 ppmv (parts per million by volume), 4.0 g cm^{-2}, and 270 Dobson, respectively. The previous LUTs only work for MERIS bands. In this work, we supplemented spectral bands configured for other sensors and recomputed the corresponding parameters in the LUTs, in order to adapt for multi-sensor data application. Several lakes near the Yangtze's mouth – East Taihu Lake, Gehu Lake, and Dianshan

Lake, where we conducted measurements of spectroradiometry and water quality for the waters – are regarded as ground known targets, assuming that the lakes have stable reflectance. Therefore, the parameters for atmospheric correction (details in Appendix 1 of Shen et al. 2010) can be determined through scanning the LUTs until the modelled R_{rs} spectra that best fit the measurements at all candidate bands are found. The applied approach is based on the assumption that the aerosol distribution is spatially stable and homogeneous in the region.

4.   Recalibration of algorithm

It might be considered that an algorithm for SPM retrieval would be relatively simple. However, applying the algorithm to turbid waters with an SPM concentration spanning two or three orders of magnitude, such as the Yangtze estuarine and adjacent coastal waters, is challenging work. Shen et al. (2010) proposed a semi-empirical radiative transfer model based on the Kubelka-Munk two-stream approximation of radiative transfer theory in water media. Remote-sensing reflectance (water-leaving reflectance) can be given by

$$R_{rs} = \frac{\alpha\beta C_{spm}}{1 + \beta C_{spm} + \sqrt{1 + 2\beta C_{spm}}}. \tag{1}$$

α and β are the fitting constants of Equation (1), which can be recalibrated and optimized by *in situ* simultaneous measurements of remote-sensing reflectance, R_{rs}, in units of inverse steradian, and the SPM concentration, C_{spm}, in units of grammes per litre (g l^{-1}), using the least squares method. The constant α has a similar function to the constant f in the Gordon model (Gordon, Brown, and Jacobs 1975). It is affected by illumination conditions and water types. β is the *ratio* of mass-specific backscattering coefficient b_b and absorption coefficient a.

In situ data of 225 reflectance values were selected for the model recalibration, in accordance with the strategy of the mean absolute percentage difference being less than 50%. The absolute percentage difference (APD) is calculated as

$$APD = ((|X_i - Y_i|)/Y_i) \times 100(\%),$$

where X is the modelled R_{rs} and Y is the *in situ* measured R_{rs}. The subscript i' represents an individual sample.

Moreover, the eligible data of reflectance should be collected under the situation of sunlight illumination (between 09:00 and 15:00), wind speed (<5 m s^{-1}), cloud coverage (<10–20%), and wave height (<2 m). The number of 144 samples available was involved in the recalibration of the semi-empirical radiative transfer model for the SPM retrieval. Two constants in the model, α and β, were wavelength-dependent and computed using the least squares non-linear regression method. Table 2 lists the two constants for multi-sensor spectral bands (>500 nm). Through statistical regression analysis for two variables, R_{rs} and C_{spm}, results showed the mean APD < 30% in visible bands and <50% in near-infrared bands, root-mean-square-error (RMSE) < 0.0085 (sr^{-1}), and the coefficient of determination (R^2) > 0.75. Figure 2 shows the fitting curves *versus* sample spaces for wavelength candidates for SPM retrieval (e.g. in 555, 620, 665, 709, 745, and 858 nm).

Table 2. The α and β constants for the MODIS, MERIS, FY-3 MERSI, and GOCI SPM algorithms in their spectral bands (>550 nm) adapted to highly turbid waters.

Sensor	Central band (nm)	α	B	APD (%)	RMSE (sr^{-1})	R^2 (%)
FY-3 (250 m)	550	0.0467	35.2459	20.2353	0.0057	75.77
MODIS (1 km)	551	0.0471	34.9441	20.2754	0.0057	75.83
GOCI	555	0.0488	33.7132	20.5207	0.0059	75.95
MERIS	560	0.0509	32.2256	20.8517	0.0062	76.18
FY-3 (1 km)	565	0.0532	30.5814	21.1969	0.0064	76.31
MERIS	620	0.0711	13.6880	26.7349	0.0081	78.22
MODIS (250 m)	645	0.0747	12.4377	27.1824	0.0082	79.12
FY-3 (250 m)	650	0.0754	12.0454	27.4604	0.0082	79.31
GOCI	660	0.0771	11.0158	29.2043	0.0084	79.22
MERIS	665	0.0779	10.7085	29.9945	0.0085	79.05
MODIS (1 km)	667	0.0779	10.6286	30.2303	0.0085	79.08
MODIS (1 km)	678	0.0793	10.3241	29.5631	0.0085	79.58
GOCI	680	0.0797	10.2475	29.2608	0.0085	79.85
MERIS	681	0.0798	10.2189	29.1862	0.0084	79.89
FY-3 (1 km)	685	0.0801	10.1105	28.9331	0.0084	80.04
MERIS	709	0.0851	07.3001	30.6066	0.0078	83.10
GOCI	745	0.0954	02.9698	39.4375	0.0057	89.35
MODIS (1 km)	748	0.0958	02.9325	39.2503	0.0057	89.48
MERIS	754	0.0976	02.8571	38.9281	0.0057	89.71
MERIS	760	0.0946	02.8887	39.6762	0.0057	89.10
FY-3 (1 km)	765	0.0978	02.8182	39.2072	0.0057	89.58
MERIS	779	0.0999	02.9285	39.1730	0.0059	89.45
MODIS (250 m)	858	0.1038	01.8042	44.2173	0.0048	91.23
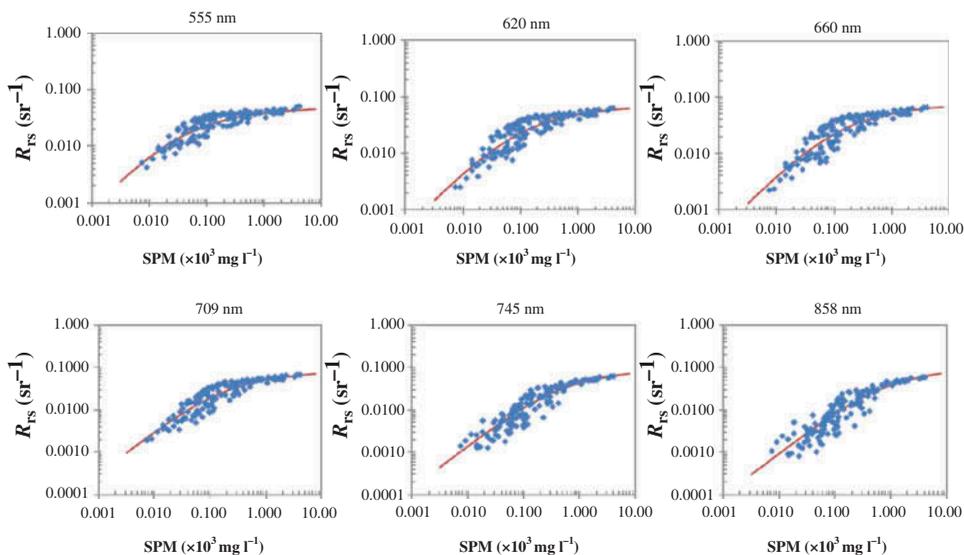
Figure 2. Non-linear regression curve for multi-sensor at six selected bands (555, 620, 660, 709, 745, and 858 nm), with 144 samples of SPM *versus* R_{rs} data on the scatter plot.
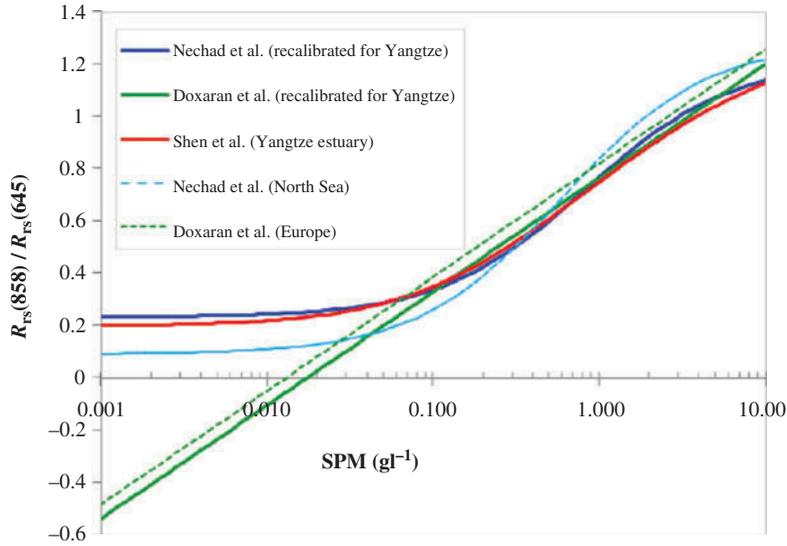
Figure 3. Non-linear relationship between SPM and ratio of $R_{rs}(858)$ to $R_{rs}(645)$. The green dashed line comes from the SPM retrieval model of Doxaran et al. (2009) and the corresponding green solid line from the same model but recalibrated by *in situ* data of the Yangtze estuary. Likewise, the blue dashed line comes from the SPM retrieval model of Nechad, Ruddick, and Park (2010) and the corresponding blue solid line from the same model but recalibrated by *in situ* data of the Yangtze estuary. The red solid line originates from the model of Shen et al. (2010).

A single band-based algorithm for SPM retrieval (Nechad, Ruddick, and Park 2010; Shen et al. 2010) can be used flexibly to adopt any spectral band sensitive to SPM. However, a band ratio-based algorithm, e.g. near-infrared to red band ratio (Doxaran *et al*. 2009), would possibly improve the accuracy of SPM retrieval, and arising from that might mitigate the effects of atmospheric path radiance due to imperfect atmospheric correction over turbid waters. However, it would perhaps lead to an underestimation of SPM and even show a negative for low SPM (e.g. < 20 mg l^{-1}) waters (see green line in Figure 3). In order to keep water-leaving reflectance signals 'sensitive' for both high and low reflective waters within one ocean scene, Shen et al. (2010) proposed an approach of wavelength switching through sensitivity analysis, for satellite retrieval of SPM with a very wide range of concentration. In this work, three bands from GOCI centred on 555, 660, and 745 nm, two bands from Terra Aqua MODIS centred on 645 and 858 nm, four bands from Envisat MERIS centred on 560, 620, 709, and 779 nm, and three bands from FY-3 MERSI centred on 560, 660, and 767 nm were selected for the SPM retrievals.

Two strategies for wavelength switching may be applied. One strategy is to set a threshold of R_{rs} in a specified wavelength for a certain range of SPM concentration, based on sensitivity of the R_{rs} to the SPM (Shen et al. 2010). Using this strategy for wavelength switching might lead to a retrieved SPM incontinuity (such as 'boundary effects') in spatial distribution. This is unlikely although sometimes it could occur. Another strategy is to select a maximum of the SPM results retrieved by R_{rs} using all retrieval wavelengths, so as to keep spatial continuity of the resulting SPM (Shen et al. 2013). This means the maximum SPM corresponds to that retrieved by the R_{rs} with the highest sensitivity.

5. Inter-comparison

5.1. *Comparison of inter-sensor products*

Four near-simultaneous images captured on 5 April 2011 from the three sensors, GOCI, Terra MODIS, and Aqua MODIS, two near-simultaneous images on 9 October 2011 from two sensors, GOCI and Envisat MERIS, and three near-simultaneous images on 30 April 2010 from three sensors, Terra MODIS, Envisat MERIS, and FY-3 MERSI, were obtained for comparative analysis of inter-sensor-derived SPM products.

It can be seen in Figure 4(*a*) and (*b*) that the SPM results from GOCI (overpass at 02:28 UTC) and Terra MODIS (overpass at 02:10 UTC) had a better correspondence in spatial distribution and magnitude. A good match mainly occurred in low and moderate SPM waters, but not in high SPM waters. The extremely high SPM waters
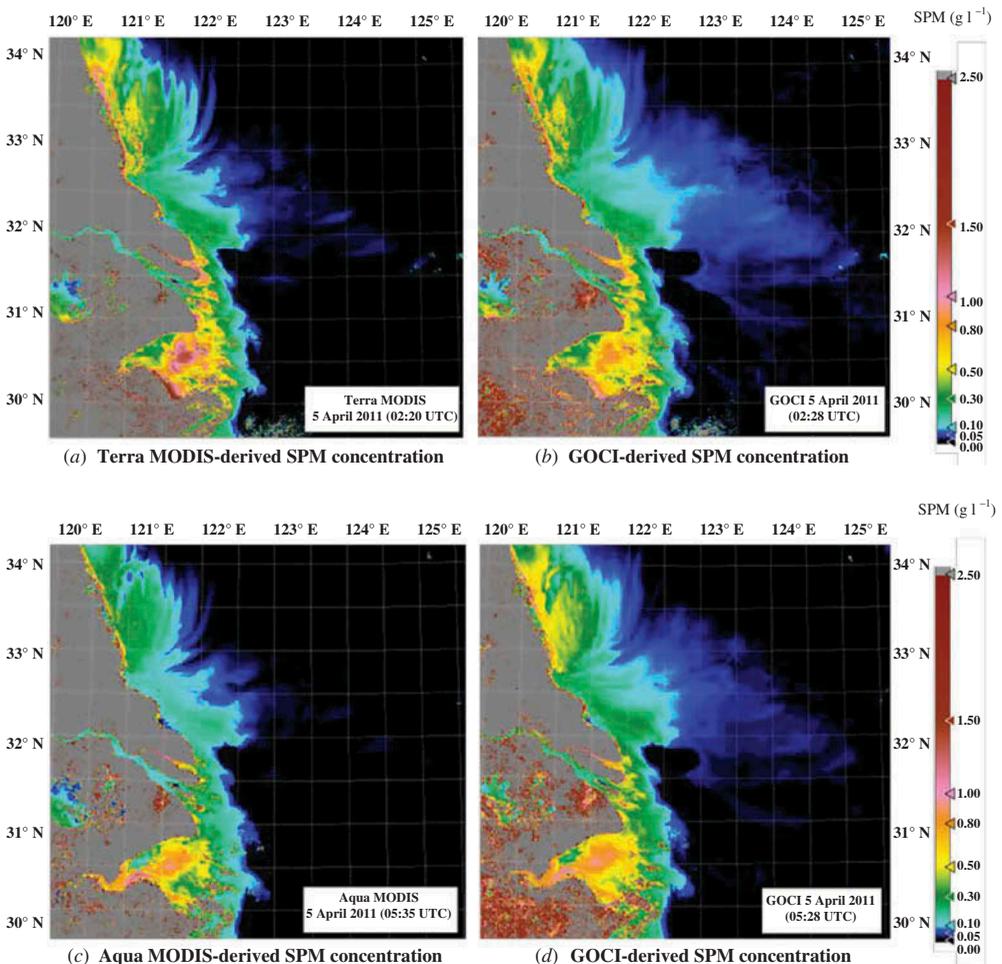
Figure 4. Two pairs of synchronous images captured on 5 April 2011, Terra MODIS-derived SPM at 2:20 UTC (*a*) *versus* GOCI-derived SPM at 2:28 UTC (*b*) and Aqua MODIS-derived SPM at 5:35 UTC (*c*) *versus* GOCI-derived SPM at 5:28 UTC (*d*). (*a*) Terra MODIS-derived SPM concentration; (*b*) GOCI-derived SPM concentration; (*c*) Aqua MODIS-derived SPM concentration; (*d*) GOCI-derived SPM concentration.
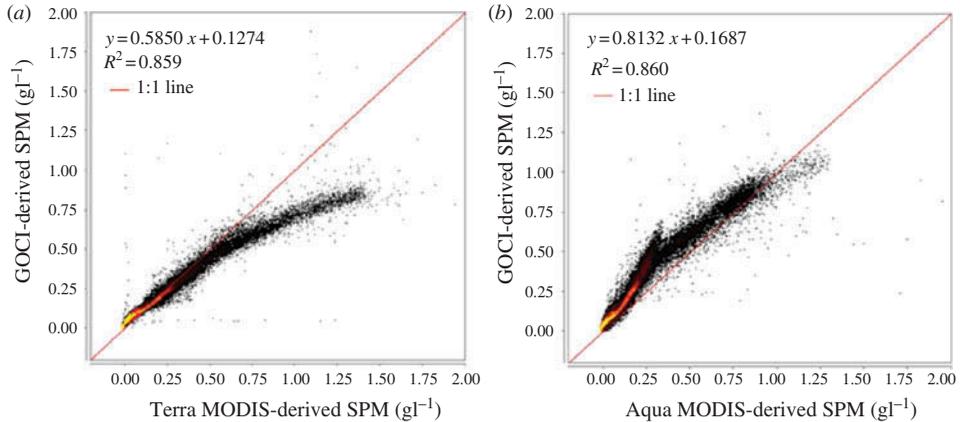
Figure 5. 1:1 scatterplots of GOCI-derived SPM at 2:28 UTC *versus* Terra MODIS-derived SPM at 2:20 UTC (*a*) and GOCI-derived SPM at 5:28 UTC *versus* Aqua MODIS-derived SPM at 5:35 UTC (*b*). Satellite data come from the same day of 5 April 2011.

mainly occurred in the centre of Hangzhou Bay, where Terra MODIS-derived SPM (up to 1.0 g l^{-1}) was higher than GOCI-derived SPM (up to 0.8 g l^{-1}). Furthermore, the 1:1 scatterplot of GOCI SPM against Terra MODIS SPM, shown in Figure 5(*a*), likewise, indicated that the Terra MODIS SPM was higher than the GOCI SPM when SPM was high (above 0.5 g l^{-1}). The regression slope and intercept were 0.585 and 0.1274 (in units of g l^{-1}), respectively.

In Figures 4(*c*) and (*d*), the SPM results from GOCI (overpass at 05:28 UTC) and Aqua MODIS (overpass at 05:35 UTC) displayed a good correspondence. The differences mainly occurred in the South Branch (e.g. 31.7° N/121.3° E) and the south of the Subei Coast (e.g. 32.2° N/122° E), where the GOCI-derived SPM was about 0.1 g l^{-1} and the Aqua MODIS-derived SPM was about 0.3 g l^{-1}. Furthermore, the 1:1 scatterplot of GOCI SPM against Aqua MODIS SPM, shown in Figure 5(*b*), indicated that the Aqua MODIS SPM was lower than the GOCI SPM when the SPM was moderate (about 0.1–0.3 g l^{-1}). The moderate SPM waters were mainly distributed in the entire South Branch and part of the Subei Coast. The regression slope and intercept were 0.8132 and 0.1687 (in units of g l^{-1}), respectively.

In Figure 6, the SPM results from GOCI (overpass at 02:28 UTC) and Envisat MERIS (overpass at 02:06 UTC), near-simultaneous images captured on 9 October 2011, were near-perfectly concordant in magnitude and spatial distribution. In both images, despite the coverage of cloud marked by white colour where the colourful scatter points might exceed 10%, the regions of interest were rarely contaminated by cloud except in the north of the Subei Coast. Likewise, the 1:1 scatterplot of GOCI SPM against Envisat MERIS SPM, shown in Figure 7, indicated that both SPMs had a good concordance (near to 1:1). The statistic regression slope and intercept were 0.9617 and 0.0041 (in units of g l^{-1}), respectively.

The SPM products retrieved from three sensors – Terra MODIS, Envisat MERIS, and FY-3 MERSI – with near-simultaneous overpass around 10:00 (local time) on 30 April 2010, combined with autonomous turbidity observations in fixed stations, are compared in Section 5.2.

(*a*) **Envisat MERIS-derived SPM concentration**   (*b*) **GOCI-derived SPM concentration**
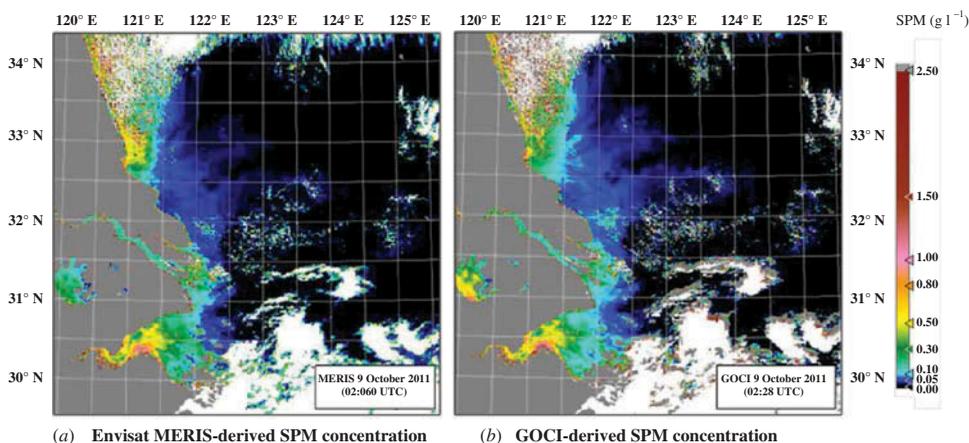
Figure 6.   One pair of synchronous images captured on 9 October 2011, GOCI-derived SPM at 2:28 UTC *versus* Envisat MERIS-derived SPM at 2:06 UTC. Envisat MERIS-derived SPM concentration; GOCI-derived SPM concentration.
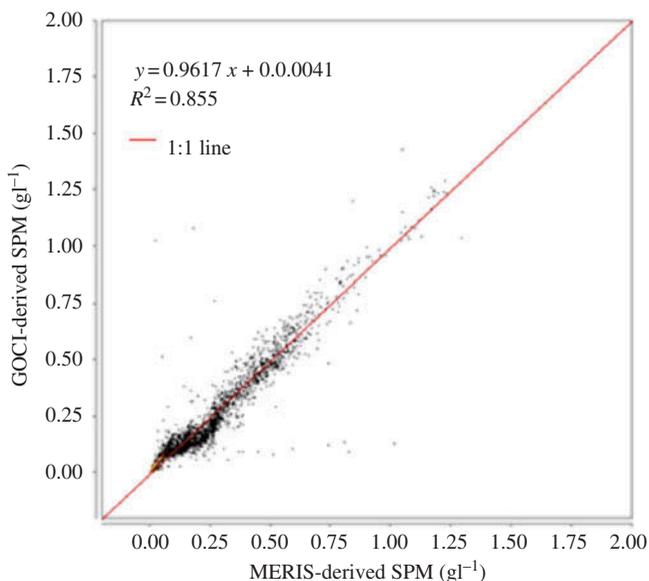
Figure 7.   1:1 scatterplot of GOCI-derived SPM at 2:28 UTC *versus* Envisat MERIS-derived SPM at 2:06 UTC.

5.2.   *Comparison of multi-sensor SPM and fixed-station observations*

Simultaneous satellite and fixed-station observations in the three days, 5 April and 9 October 2011 and 30 April 2010, were selected for the inter-comparison of the SPM products from different sources. Satellite SPM values in the fixed stations, through picking 5 × 5 pixel-boxes around the Chongxi and Nanmen sites, and 3 × 3 pixel-boxes around the Baozhen site, due to its relatively small area, were statistically calculated with arithmetic mean and standard deviation (SD).
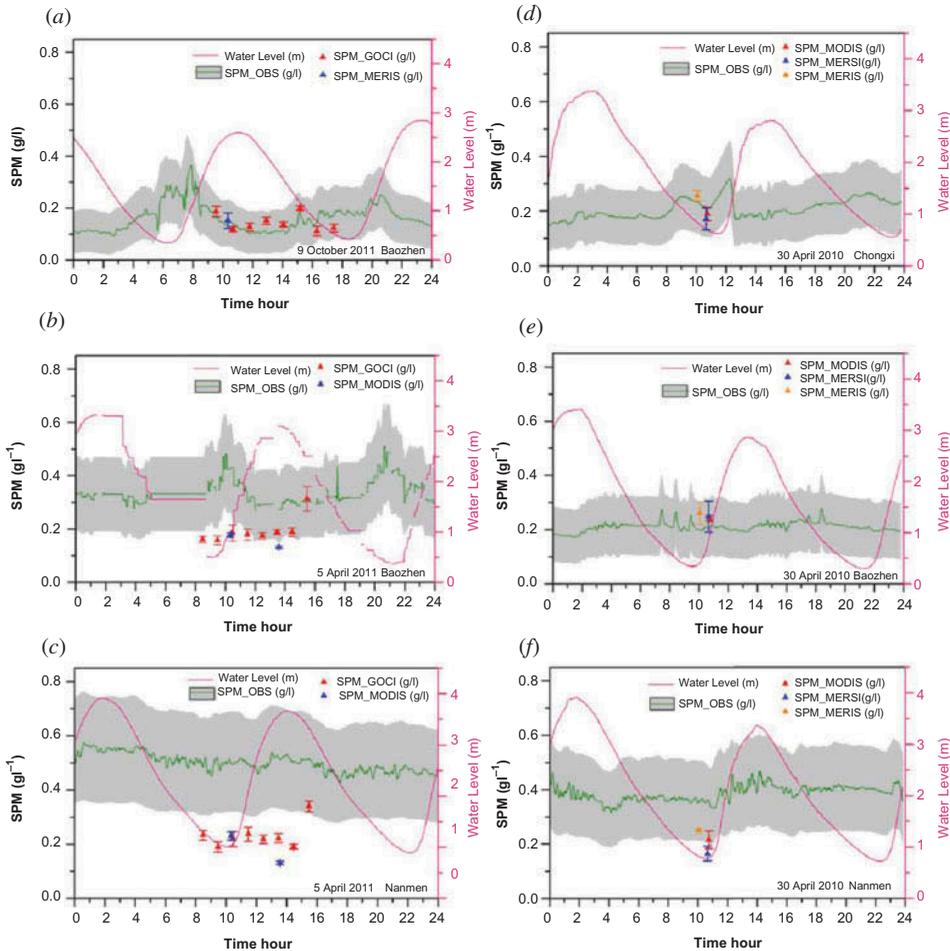
Figure 8. Synchronous multi-sensor satellite-derived SPM products with concurrent OBS SPM (arithmetic mean: green line; standard deviation: grey zone) and water level data (pink line) in three field fixed stations. The OBS SPM originated from autonomous measurements for turbidity by the OBS. On 9 October 2011, there were eight data from GOCI-derived SPM between 0:28 and 7:28 UTC and single data of Envisat MERIS-derived SPM in Baozhen (a). On 5 April 2011, there were eight data from GOCI-derived SPM between 0:28 and 7:28 UTC and two data of Terra/Aqua MODIS-derived SPM in Baozhen (b) and Nanmen (c). On 30 April 2010, there were the triplets of Terra MODIS (02:45 UTC), Envisat MERIS (02:04 UTC), and FY-3 MERSI (02:40 UTC)-derived SPM products in Chongxi (d), Baozhen (e), and Nanmen (f).

On 9 October 2011, MERIS SPM (0.151 g l^{-1} at 10: 20 local time) was close to GOCI SPM (0.138 g l^{-1} at 10:28 local time) in Baozhen (see Figure 8(a)). They both showed perfect accordance. One MERIS-derived SPM (blue triangle) with eight GOCI-derived SPM (red triangles) on that day were in a good correspondence with the OBS SPM (green line: arithmetic mean; grey zone: standard deviation). The confidence of the good match also originated from the validation of MERIS-retrieved SPM products using the proposed algorithm *versus in situ* ship-based measurements (re. Shen et al. 2010). This implies that the SPM algorithm can be applied to GOCI, although the MERIS and GOCI bands used for the SPM retrieval are not completely the same. However, for turbid waters with a wide

range of SPM concentration, three bands at least, located in the green, red, and near-infrared spectral range, should be appropriate for SPM retrieval.

On 5 April 2011, GOCI SPM values had a range between 0.158 and 0.313 g l^{-1} in Baozhen (Figure 8(*b*)) and between 0.189 and 0.339 g l^{-1} in Nanmen (Figure 8(*c*)). Sudden increases in the SPM of up to 0.313 g l^{-1} in Baozhen and up to 0.339 g l^{-1} in Nanmen occurred at 15:28 local time, which were possibly affected by atmospheric correction due to solar elevation decrease and atmospheric path radiance increase at that time. GOCI SPM (0.185 g l^{-1} at 10:28 local time) against Terra MODIS SPM (0.177 g l^{-1} at 10:20 local time) in Baozhen, and GOCI SPM (0.219 g l^{-1} at 10:28 local time) against Terra MODIS SPM (0.230 g l^{-1} at 10:20 local time) in Nanmen, were both in a good accordance, whereas Aqua MODIS SPM (0.132 g l^{-1} at 13:35 local time) was a bit lower than GOCI SPM (0.189 g l^{-1} at 13:28 local time) in Baozhen, and Aqua MODIS SPM (0.131 g l^{-1} at 13:35 local time) was obviously lower than GOCI SPM (0.222 g l^{-1} at 13:28 local time) in Nanmen. Figure 8(*b*) shows that multi-sensor-derived SPM in Baozhen, overall, was slightly lower than the OBS SPM but was still in a reasonable range. Anomalously, the OBS SPM in Nanmen was mostly higher than multi-sensor-derived SPM (Figure 8(*c*)). Further analysis showed that the mean OBS SPM in Nanmen was 0.304 g l^{-1} (SD: 0.043 g l^{-1}) in March 2011 and 0.167 g l^{-1} (SD: 0.048 g l^{-1}) in May 2011. The sharply increased OBS SPM (0.5 g l^{-1} on average) in April 2011 was speculated to have arisen from the OBS sensor in Nanmen, which had been contaminated by biogenic and chemical materials.

On 30 April 2010, the triplets of multi-sensor SPM products in Chongxi, Baozhen, and Nanmen sites were compared (Figure 8(*d–f*)), respectively. The first triplet (Figure 8(*d*)) was Terra MODIS SPM of 0.189 g l^{-1} (at 10:45 local time, red triangle), FY-3 MERSI SPM of 0.172 g l^{-1} (at 10:40 local time, blue triangle), and Envisat MERIS SPM of 0.255 g l^{-1} (at 10:04 local time, orange triangle) in Chongxi, with a mean difference of 0.056 g l^{-1}. The second triplet (Figure 8(*e*)) was Terra MODIS SPM of 0.241 g l^{-1}, FY-3 MERSI SPM of 0.248 g l^{-1}, and Envisat MERIS SPM of 0.261 g l^{-1} in Baozhen, with the least difference of 0.013 g l^{-1}. The third triplet (Figure 8(*f*)) was Terra MODIS SPM of 0.215 g l^{-1}, FY-3 MERSI SPM of 0.165 g l^{-1}, and Envisat MERIS SPM of 0.251 g l^{-1} in Nanmen, with a mean difference of 0.057 g l^{-1}. An inter-comparison for the three triplets of multi-sensor-derived SPM displayed good accordance. The three triplets of multi-sensor SPM products were in a good correspondence with the OBS SPM, especially in the Chongxi and Baozhen sites.

6. Discussions

For highly reflective waters, SPM retrieval using shorter wavelengths (e.g. blue or green wavelengths) will lead to optical 'saturation' phenomena due to lower pure water absorption (Nechad, Ruddick, and Park 2010; Shen et al. 2010). This implies that retrieval wavelengths selected should move to longer wavelengths (e.g. red or near-infrared wavelengths) for high SPM (Nechad, Ruddick, and Park 2010; Doxaran et al. 2009). For waters with a very wide range of SPM between 10° and 10^{3} of magnitude (mg l^{-1}), Shen et al. (2010) proposed a strategy of wavelength switching for the SPM retrieval, as a compromise solution of avoiding saturation in high reflectance and degradation of accuracy in low reflectance. Regarding the possible occurrence of the retrieved SPM spatial incontinuity using R_{rs} thresholds, Shen et al. (2013) also proposed another strategy that preferred a maximum of the SPM results retrieved by R_{rs} using all retrieval wavelengths.
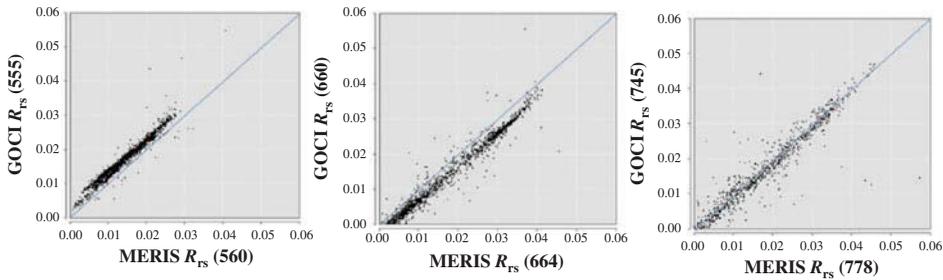
Figure 9.　1:1 scatterplots of three pairs of remote-sensing reflectance: MERIS R_{rs}(560) *versus* GOCI R_{rs}(555), MERIS R_{rs}(660) *versus* GOCI R_{rs}(664), and MERIS R_{rs}(778) *versus* GOCI R_{rs}(745).

The proposed semi-empirical radiative transfer model for SPM retrieval is physically based, although it depends on the accuracy of atmospheric correction to some extent, similar to other single-band-based algorithms. If using near-infrared to red band ratio, from two algorithms of Nechad, Ruddick, and Park (2010) and Shen et al. (2010), respectively, very similarly modelled curves were found in Figure 3. Moreover, both algorithms stay within the physically possible bounds, e.g. when SPM is lower.

By applying our proposed algorithm to five sensors, it was found that near-simultaneous GOCI and Envisat MERIS-derived SPM products were near-perfectly consistent in the whole Yangtze estuary and Hangzhou Bay, Yellow Sea, and East China Sea (Figures 6–7). The consistency originated from both having compatible spectral bands for retrieval as well as approximate remote-sensing reflectance at the corresponding bands. It is shown in Figure 9 that three pairs of remote-sensing reflectance: MERIS R_{rs} (560) *versus* GOCI R_{rs} (555), MERIS R_{rs} (660) *versus* GOCI R_{rs} (664), and MERIS R_{rs} (778) *versus* GOCI R_{rs} (745) have a near 1:1 correspondence. The slight difference possibly results from different spectral band settings (location and width).

An obvious discrepancy occurred mainly in the high SPM pixels of GOCI-derived SPM *versus* Terra MODIS-derived SPM (Figures 4(*a–b*) and 5(*a*)), and in the moderate SPM pixels of GOCI SPM *versus* Aqua MODIS SPM (Figures 4(*c–d*) and 5(*b*)). This possibly arose from different retrieval bands employed for the retrieval. Only two bands with relatively coarse spectral intervals, centred at 645 and 858 nm, were used, compared to GOCI using three bands for the retrieval. Moreover, the Aqua MODIS SPM was lower than the GOCI SPM in low and moderate SPM waters (Figure 5(*b*)), which was possibly caused by the absence of an Aqua MODIS green band employed for retrieval. In addition, it was found that the Aqua MODIS remote-sensing reflectance at 678 nm was 0.004 sr^{-1} on average lower when compared with the GOCI remote-sensing reflectance at 660 nm (the result is not shown). A similar result by Ruddick et al. (2012) found that Aqua MODIS reflectance was possibly lower than GOCI reflectance in low reflective pixels, when comparing three pairs of remote-sensing reflectance: GOCI R_{rs} (443) *versus* Aqua MODIS R_{rs} (443), GOCI R_{rs} (555) *versus* Aqua MODIS R_{rs} (555), and GOCI R_{rs} (680) *versus* Aqua MODIS R_{rs} (678), in the Baohai Sea. The difference, likewise, would result in a corresponding bias in SPM products. Other discrepancies highlight the need for further investigation that is beyond the scope of this article.

Autonomous measurements for OBS turbidity in fixed field stations may increase the opportunity to validate satellite retrieval products. The SPM concentration (dry-mass weight per volume) is generally proportional to the OBS turbidity (NTU). However, the

calibrated relationship between the OBS turbidity and the corresponding SPM concentration has not been stable and can be impacted by particle size, shape, and composition, aggregation/flocculation, bubbles, and chemical and biological fouling. The unknown time variation in particle size or aggregation/flocculation and fouling will nearly always result in inaccurate OBS data (Downing 2006). An effective way to develop the calibrated relationship is by simultaneous operation of OBS measurements and water samplings, which may minimize the physical and biochemical impacts. However, the way is impractical for the autonomous measurements due to inaccessibility, remote operations, and limited technical support.

Although the three OBS instruments were of the same type, the difference in their purchase and time use would affect the discrepancy in calibration coefficients. Nevertheless, we adopted two calibrated relationships, one from our cruise campaign in the Yangtze river mouth during July 2011 and another from the calibration in the South Branch by Xue, He, and Wang (2004), for OBS calibration. The results suggested that satellite multi-sensor-derived SPM was mostly in good correspondence with the OBS SPM time series in the three fixed stations on 9 October and 5 April 2011 and 30 April 2010 (Figure 8), except in the Nanmen station on 5 April 2011 (Figure 8(*c*)). In addition, since the three fixed stations were located in the upper estuary, the OBS SPM with a flat variation in a day should be normal, unlike the strong fluctuations in the Turbidity Maximum and Hangzhou Bay. Hence, it is no surprise that there is a flat trend in the GOCI time series SPM in these stations (Figure 8(*a*–*c*)).

7. Conclusion

The proposed SPM algorithm was recalibrated using a dataset of 144 samples measured *in situ* from 17 cruise campaigns. The algorithm has become more generic and adapted for multi-sensor retrievals. The LUTs for atmospheric correction, which were only for MERIS data in previous work, were supplemented and are currently suitable for multi-sensor data. Through comparative analysis of inter-sensor-derived products, it was found that GOCI-derived SPM with Envisat MERIS-derived SPM was in a near-perfect accordance in the entire Yangtze estuary and Hangzhou Bay, Yellow Sea, and East China Sea. Likewise, Envisat MERIS-, Terra MODIS-, and FY-3 MERSI-derived SPM products exhibited a good accordance in three fixed stations in the Yangtze estuary. Terra MODIS-derived SPM with GOCI-derived SPM, except in Hangzhou Bay (i.e. high SPM waters), and Aqua MODIS-derived SPM with GOCI-derived SPM, except in the South Branch and south of the Subei coast (i.e. moderate SPM waters), showed a good correspondence. These imply that the SPM retrieval algorithm proposed can be applied to multiple sensors. Results suggest that the algorithm is feasible and compatible for SPM retrieval by multiple sensors. Matchups of synchronous multi-sensor-derived SPM with concurrent OBS SPM time series observed in three field fixed stations mostly displayed a good correspondence. This will enhance future confidence to further validate time series SPM products estimated from satellite multi-sensors.

Funding

References

Brajard, J., C. Jamet, C. Moulin, and S. Thiria. 2006. "Use of A Neuro-Variational Inversion for Retrieving Oceanic and Atmospheric Constituents from Satellite Ocean Colour Sensor: Application to Absorbing Aerosols." *Neural Networks* 19: 178–185. doi:10.1016/j.neunet.2006.01.015.

Choi, J., Y. J. Park, J. H. Ahn, H. Lim, J. Eom, and J. Ryu. 2012. "GOCI, the World's First Geostationary Ocean Color Observation Satellite, for the Monitoring of Temporal Variability in Coastal Water Turbidity." *Journal of Geophysical Research: Oceans* 117: C09004. doi:10.1029/2012JC008046.

Cui, T., J. Zhang, S. Groom, L. Sun, T. Smyth, and S. Sathyendranath. 2010. "Validation of MERIS Ocean-Color Products in the Bohai Sea: A Case Study for Turbid Coastal Waters." *Remote Sensing of Environment* 114 (10): 2326–2336. doi:10.1016/j.rse.2010.05.009.

Donlon, C., B. Berruti, A. Buongiorno, M.-H. Ferreira, P. Féménias, J. Frerick, P. Goryl, U. Klein, H. Laur, C. Mavrocordatos, J. Nieke, H. Rebhan, B. Seitz, J. Stroede, and R. Sciarra. 2012. "The Global Monitoring for Environment and Security (GMES) Sentinel-3 Mission." *Remote Sensing of Environment* 120: 37–57. doi:10.1016/j.rse.2011.07.024.

Downing, J. 2006. "Twenty-Five Years with OBS Sensors: the Good, the Bad, and the Ugly." *Continental Shelf Research* 26: 2299–2318. doi:10.1016/j.csr.2006.07.018.

Doxaran, D., J. M. Froidefond, P. Castaing, and M. Babin. 2009. "Dynamics of the Turbidity Maximum Zone in a Macrotidal Estuary (The Gironde, France): Observations from Field and MODIS Satellite Data." *Estuarine, Coastal and Shelf Science* 81: 321–332. doi:10.1016/j.ecss.2008.11.013.

El-Asmar, H. M., and K. White. 2002. "Changes in Coastal Sediment Transport Processes Due to Construction of New Damietta Harbour, Nile Delta, Egypt." *Coastal Engineering* 46: 127–138. doi:10.1016/S0378-3839(02)00068-6.

Fargion, G. S., and J. L. Muller, 2000, "Ocean Optics Protocols for Satellite Ocean Color Sensor Validation, Revision2." NASA TM-2000-209966, GSFC, 2000. http://seabass.gsfc.nasa.gov/docs/SIMBIOS-OOPR2.pdf

Gordon, H. R., O. B. Brown, and M. M. Jacobs. 1975. "Computed Relationships Between the Inherent and Apparent Optical Properties of a Flat Homogeneous Ocean." *Applied Optics* 14 (2): 417–427.

Gregg, W. W., and R. H. Woodward. 1998. "Improvements in Coverage Frequency of Ocean Color: Combining Data from Seawifs and MODIS." *IEEE Transactions on Geoscience and Remote Sensing* 36: 1350–1353. doi:10.1109/36.701084.

IOCCG (International Ocean-Color Coordinating Group) 2000. "Remote Sensing of Ocean Color in Coastal, and Other Optically-Complex, Waters." In *Reports of the International Ocean-Color Coordinating Group*, edited by S. Sathyendranath. Dartmouth: IOCCG.

IOCCG (International Ocean-Color Coordinating Group) 2007. "Ocean-Colour Data Merging." In *Reports of the International Ocean-Colour Coordinating Group*, edited by W. Gregg. Dartmouth: IOCCG.

IOCCG (International Ocean-Color Coordinating Group) 2008. "Why Ocean Colour? The Societal Benefits of Ocean-Colour Technology." In *Reports of the International Ocean-Colour Coordinating Group*, edited by T. Platt, N. Hoepffner, V. Stuart, and C. Brown. Dartmouth: IOCCG.

IOCCG (International Ocean-Color Coordinating Group) 2010. "Atmospheric Correction for Remotely-Sensed Ocean-Colour Products." In *Reports of the International Ocean-Colour Coordinating Group*, edited by M. Wang. Dartmouth: IOCCG.

Jamet, C., S. Thiria, C. Moulin, and M. Crepon. 2005. "Use of A Neurovariational Inversion for Retrieving Oceanic and Atmospheric Constituents from Ocean Color Imagery: A Feasibility

Study." *Journal of Atmospheric and Oceanic Technology* 22: 460–475. doi:10.1175/JTECH1688.1.

Krause-Jensen, D., and K. Sand-Jensen. 1998. "Light Attenuation and Photosynthesis of Aquatic Plant Communities." *Limnology and Oceanography* 43: 396–407. doi:10.4319/lo.1998.43.3.0396.

Maritorena, S., O. H. Fanton d'Andon, A. Mangin, and D. A. Siegel. 2010. "Merged Satellite Ocean Color Data Products Using a Bio-Optical Model: Characteristics, Benefits and Issues." *Remote Sensing of Environment* 114: 1791–1804. doi:10.1016/j.rse.2010.04.002.

Maritorena, S., and D. A. Siegel. 2005. "Consistent Merging of Satellite Ocean Color Data Sets Using a Bio-Optical Model." *Remote Sensing of Environment* 94 (4): 429−440. doi:10.1016/j.rse.2004.08.014.

McClain, C. R. 2009. "A Decade of Satellite Ocean Color Observations." *Annual Review of Marine Science* 1: 19–42. doi:10.1146/annurev.marine.010908.163650.

Miller, R. L., and B. A. McKee. 2004. "Using MODIS Terra 250 M Imagery to Map Concentrations of Total Suspended Matter in Coastal Waters." *Remote Sensing of Environment* 93: 259–266. doi:10.1016/j.rse.2004.07.012.

Mobley, C. D. 1999. "Estimation of the Remote-Sensing Reflectance from Above-Surface Measurements." *Applied Optics* 38: 7442–7455. doi:10.1364/AO.38.007442.

Morel, A., Y. Huot, B. Gentili, P. J. Werdell, S. B. Hooker, and B. A. Franz. 2007. "Examining the Consistency of Products Derived from Various Ocean Color Sensors in Open Ocean (Case 1) Waters in the Perspective of A Multi-Sensor Approach." *Remote Sensing of Environment* 111 (1): 69–88. doi:10.1016/j.rse.2007.03.012.

Nechad, B., K. Ruddick, and Y. Park. 2010. "Calibration and Validation of A Generic Multisensor Algorithm for Mapping of Total Suspended Matter in Turbid Waters." *Remote Sensing of Environment* 114: 854–866. doi:10.1016/j.rse.2009.11.022.

Pottier, C., V. Garcon, G. Larnicol, J. Sudre, P. Schaeffer, and P. Y. Le Traon. 2006. "Merging Seawifs and MODIS/AQUA Ocean Color Data in North and Equatorial Atlantic Using Weighted Averaging and Objective Analysis." *IEEE Transactions on Geoscience and Remote Sensing* 44 (11): 3436–3451. doi:10.1109/TGRS.2006.878441.

Ruddick, K., Q. Vanhellemont, J. Yan, G. Neukermans, G. Wei, and S. Shang. 2012. "Variability of Suspended Particulate Matter in the Bohai Sea from the Geostationary Ocean Color Imager (GOCI)." *Ocean Science Journal* 47 (3): 331–345. doi:10.1007/s12601-012-0032-4.

Ryu, J., H. Han, S. Cho, Y. Park, and Y. Ahn. 2012. "Overview of Geostationary Ocean Color Imager (GOCI) and GOCI Data Processing System (GDPS)." *Ocean Science Journal* 47 (3): 223–233. doi:10.1007/s12601-012-0024-4.

Schoellhamer, D. H., T. E. Mumley, and J. E. Leatherbarrow. 2007. "Suspended Sediment and Sediment-Associated Contaminants in San Francisco Bay." *Environmental Research* 105: 119–131. doi:10.1016/j.envres.2007.02.002.

Schroeder, T., I. Behnert, M. Schaale, J. Fischer, and R. Doerffer. 2007. "Atmospheric Correction Algorithm for MERIS above Case-2 Waters." *International Journal of Remote Sensing* 28: 1469–1486. doi:10.1080/01431160600962574.

Shen, F., and W. Verhoef. 2010. "Suppression of Local Haze Variations in MERIS Images over Turbid Coastal Waters for Retrieval of Suspended Sediment Concentration." *Optics Express*, 18 (12): 12653–12662. doi:10.1364/OE.18.012653.

Shen, F., W. Verhoef, Y. Zhou, M. S. Salama, and X. Liu. 2010. "Satellite Estimates of Wide-Range Suspended Sediment Concentrations in Changjiang (Yangtze) Estuary Using MERIS Data." *Estuaries and Coasts* 33: 1420–1429. doi:10.1007/s12237-010-9313-2.

Shen, F., Y. Zhou, J. Li, Q. He, and W. Verhoef. 2013. "Remotely Sensed Variability of the Suspended Sediment Concentration and Its Response to Decreased River Discharge in the Yangtze Estuary and Adjacent Coast." *Continental Shelf Research* 69: 52–61. doi:10.1016/j.csr.2013.09.002.

Sun, L., M. H. Guo, N. Xu, L. J. Zhang, J. J. Liu, X. Q. Hu, Y. Li, Z. G. Rong, and Z. H. Zhao. 2012. "On-Orbit Response Variation Analysis of FY-3 MERSI Reflective Solar Bands Based on Dunhuang Site Calibration." *Spectroscopy and Spectral Analysis* 32 (7): 1869.

Wang, M., S. Son, and W. Shi. 2009. "Evaluation of MODIS SWIR and NIR-SWIR Atmospheric Correction Algorithms using Seabass Data." *Remote Sensing of Environment* 113: 635–644. doi:10.1016/j.rse.2008.11.005.

Xue, Y.-Z., Q. He, and Y.-Y. Wang. 2004. "The Method and Application of OBS in the Measurement of Sediment Concentration." *Journal of Sediment Research* 4: 56–60. [in Chinese with English abstract.]

Yang, C.-S., and J.-H. Song. 2012. "Geometric Performance Evaluation of the Geostationary Ocean Color Imager." *Ocean Science Journal* 47 (3): 235–246.